J Mater Sci (2007) 42:5570–5575
DOI 10.1007/s10853-006-0992-9

Microstructure and properties of an electroconductive SiC-based composite

Diletta Sciti · Andrea Balbo · Cesare Melandri · Giuseppe Pezzotti

Received: 17 November 2005 / Accepted: 22 September 2006 / Published online: 4 April 2007
© Springer Science+Business Media, LLC 2007

Abstract In this work, an SiC-based electroconductive composite is obtained through simultaneous addition of $MoSi_2$ and ZrB_2 particles. The composite material is fully densified by hot pressing at 1860 °C and the microstructure is investigated by SEM-EDS analysis. Microstructural features and mechanical properties are compared to those of a monolithic hot-pressed SiC material. The $MoSi_2$ and ZrB_2 particles, besides increasing the electrical conductivity of the silicon carbide matrix, also act as reinforcement for the material. Room-temperature strength reaches the value of 850 MPa and the fracture toughness is 4.2 MPa $m^{0.5}$. The composite electrical resistivity is of the order of 10^{-3} Ω cm.

Introduction

Silicon-carbide-based ceramics are promising materials for applications in gas turbine components, heat exchangers, and wear-resistant components. Most of these applications require good strength and toughness, high thermal conductivity and good environmental stability at high temperature. Although silicon carbide can fulfill all these requirements, one major problem is that SiC hardly densifies without additives, because of the covalent nature of Si–C bonding and the low self-diffusion coefficient. In the last decade, liquid-phase sintering has been widely studied as a viable process for obtaining dense and fine materials without excessively high temperatures and pressures [1–6].

Materials with improved sinterability and good room-temperature strength (~700 MPa) were obtained by careful optimization of the processing, sintering additives and sintering cycles [3, 7]. However, the major problems encountered with this class of liquid-phase sintered materials are the low fracture toughness and the degradation of strength at high temperature. The relatively low toughness (3 MPa $m^{0.5}$) is caused by a fine equiaxed microstructure, which does not provide any crack deflection or crack bridging phenomena. On the other hand, the high-temperature strength is degraded by the softening of residual secondary phases deriving from the sintering aids.

Furthermore, SiC-based components must be diamond-machined, due to their low electrical conductivity. Diamond machining is a costly process, which also implies limitations on the complexity of the final shapes. The addition of electroconductive phases to insulating ceramics in suitable amounts is a straightforward strategy to overcome this problem [8], since it allows components to be machined by electro-discharge machining. All these considerations have led to the attempt to fabricate electroconductive SiC-based materials with improved mechanical properties. For this aim, the silicon carbide matrix was simultaneously added with $MoSi_2$ and ZrB_2 particles. $MoSi_2$ has been coupled to several ceramic matrixes, such as Si_3N_4, SiC, SiAlON, AlN and it has been found that its addition causes a significant improvement in the mechanical properties [8–10] and the oxidation resistance [11–13].

D. Sciti (✉) · A. Balbo · C. Melandri
CNR-ISTEC, Institute of Science and Technology for Ceramics, Via Granarolo 64, 48018 Faenza, Italy
e-mail: dile@istec.cnr.it

G. Pezzotti
Department of Chemistry and Materials Technology, Kyoto Institute of Technology, Sakyo-ku, Matsugasaki, 606-8585 Kyoto, Japan

D. Sciti · G. Pezzotti
Research Institute for Nanoscience (RIN), Kyoto Institute of Technology, Sakyo-ku, Matsugasaki, 606-8585 Kyoto, Japan

As a drawback, the addition of $MoSi_2$ to SiC is expected to cause a decrease of hardness, due to its intrinsic low hardness, and of the Young's modulus, mainly because the starting $MoSi_2$ powders are always contaminated by significant amounts of silica. ZrB_2 is a very hard and stiff phase and was already found to cause an increase in fracture toughness when added to silicon carbide [14]. Both $MoSi_2$ and ZrB_2 are good electrical conductors, with resistivity of $\sim 2 \times 10^{-5}$ Ω cm.

In this contribution, the microstructure and properties of the reinforced composite are presented and compared to that of a reference liquid-phase-sintered SiC material.

Experimental

The materials of the present work were produced from commercial powders: SiC Starck BF-12: 97% β-SiC and 3% α-SiC, s. s. a. 11.6 m^2/g, silica ~1.65 wt% (estimated from the amount of oxygen); ZrB_2 Grade B (H.C. Starck, Germany), impurities (max. content): C: 0.25 wt%, O: 2 wt%, N: 0.25 wt%, Fe: 0.1 wt%, Hf: 0.2 wt%, grain size range 0.1–8 μm; $MoSi_2$ (Aldrich, Germany), <2 μm, mean particle size 1 μm and oxygen content 1 wt%.

The following compositions were prepared:

SiC + 6 wt% Al_2O_3 + 4 wt% Y_2O_3, labeled as SAY (monolithic silicon carbide);

SAY + 14 vol% $MoSi_2$ + 14 vol%ZrB_2, labeled as SZM (electroconductive composite).

The SAY powder mixture was processed using a pulsed ultrasonic method in ethyl alcohol, drying at 80 °C in a rotary evaporator and sieving through a 60-mesh screen size. The powder was densified through hot pressing at 1870 °C, 30 MPa, for 20–60 min. For the SZM composite, the powder mixture was milled for 24 h in absolute ethanol using Si_3N_4 milling media, then subsequently dried in a rotary evaporator and sieved through a 60-mesh screen size. The hot pressing was carried out at 1860°C, 30 MPa for 12 min.

The final densities were measured by the Archimedes method. Crystalline phases were identified by X-ray diffraction (Siemens D500, Germany). The microstructures were analyzed using scanning electron microscopy (SEM, Cambridge S360) and energy dispersive spectroscopy (EDS, INCA Energy 300, Oxford Instruments, UK) on polished surfaces. For this purpose, the specimens were polished with diamond paste to 0.25 μm.

Vickers microhardness (HV1.0) was measured with a load of 9.81 N, using a Zwick 3212 tester. Young's modulus (E) was measured by the resonance frequency method on $28 \times 8 \times 0.8$ mm^3 specimens using a Hewlett Packard gain-phase analyzer. Fracture toughness (K_{Ic}) was evaluated using the chevron-notched beam (CNB) in flexure. The test bars, $25 \times 2 \times 2.5$ mm^3 (length × width × thickness, respectively), were notched with a 0.08 mm diamond saw; the chevron-notch tip depth and average side length were about 0.12 and 0.80 of the bar thickness, respectively. The flexural tests were performed on a semi-articulated silicon carbide four-point jig with a lower span of 20 mm and an upper span of 10 mm on a universal screw-type testing machine (Instron mod. 6025). The specimens were deformed with a crosshead speed of 0.05 mm/min. The ''slice model'' equation of Munz et al. [15] was used to calculate K_{Ic}. On the same machine and with the same flexural jig, the flexural strength (σ), up to 1300 °C in air, was measured on chamfered bars $25 \times 2.5 \times 2$ mm^3 (length × width × thickness, respectively), using a crosshead speed of 0.5 mm/min. For the high-temperature tests, a soaking time of 18 min was set to reach thermal equilibrium. Five specimens were used for each temperature point.

The electrical resistivity measurements were carried out by a four-probe DC method at room temperature, inducing a current in bar specimens of 2 x 2.5 x 25 mm^3. The current and the voltage reading were detected at the same time in two different digital high-resolution multimeters. The resistivity values were determined from the electrical resistance measurement, taking into account the distance between the test leads and the cross-sectional area of the samples.

Results and discussion

Densification behavior

The hot-pressed SiC materials approached the theoretical density (see Table 1). Densification occurred through liquid-phase sintering, owing to the liquid formed by reaction between sintering aids and the SiO_2 present as oxidation product in the starting SiC powder. Al_2O_3, SiO_2 and Y_2O_3 can have eutectic temperatures in the 1400–1800 °C range, depending on their relative amounts [16]. The addition of $MoSi_2$ and ZrB_2 particles did not hinder densification with respect to the reference material. The

Table 1 Processing conditions, final densities and microstructural parameters

Sample label	Hot pressing conditions	Final relative density (%)	SiC mean grain size (μm)	SiC grain size distribution (μm)
SAY	1870 °C/ 38 min	98.5	0.6	0.1–2
SZM	1860 °C/ 10 min	98.0	0.4	0.1–1

comparison of the shrinkage curves (not shown) evidenced that the two systems started densification at nearly the same temperature, 1490 and 1450°C, for SAY and SZM respectively. However, for the SAY material, the relative density at the maximum temperature was only 73%, whilst in the SZM composite, the relative density at the maximum temperature was significantly higher, i.e. 95%. This indicates that densification was somewhat improved in the reinforced composite. This is likely due to the introduction of significant amounts of SiO_2 and B_2O_3, which are the surface oxides of the $MoSi_2$ and the ZrB_2 particles. Besides the Al_2O_3–Y_2O_3–SiO_2 liquid, a borosilicate phase could also have formed, during sintering. According to the B_2O_3–SiO_2 phase diagram [17], a liquid borosilicate phase forms at temperatures in the 500–1600 °C range, depending on their relative amounts.

Microstructural features

The crystalline phases revealed by X-ray diffraction in the SAY material are mainly β-SiC, crystalline YAG, and traces of α-SiC 6H and 4H polytypes, already present in the starting powders. Silicon carbide grains were preferentially etched away from polished cross-sections, thus microstructures are delineated by grain boundary phases (see Fig. 1). Grain morphology is mainly equiaxed with grain size distribution ranging from 0.1 to 2 μm and the mean grain size of ~500 nm. Adjacent SiC grains are most often separated by a thin grain boundary film, which is a residue of the liquid-phase sintering medium. The major part of the intergranular phases appears at three- and four-grain pockets, and contains Si–Al–O or Y–Si–Al–O [4, 7]. Also, the EDS analysis reveals that the composition of the phase located at triple points or in randomly distributed pockets, approaches that of the crystalline $Y_3Al_5O_{12}$-phase (YAG). According to the HRTEM studies [18], carried out on the same material presented in this work, triple pockets can be completely amorphous or partially crystalline and partially amorphous.

The main crystalline phases found in the SZM composite were the starting ones: β-SiC, $MoSi_2$, and ZrB_2, Fig. 2. Traces of minor crystalline phases were also detected, which most probably belong to α-SiC, MoB and YAG phase. Apart from the hypothesized presence of MoB, no reaction occurred among SiC, $MoSi_2$, and ZrB_2. The microstructure of the composite is revealed by fracture and polished surfaces in Figs. 3 and 4a-b. The fracture mode (Fig. 3) in the SiC matrix is mainly intergranular. In contrast, for $MoSi_2$ and or ZrB_2 particles, the fracture can be both intergranular and transgranular (Fig. 3). In Fig. 4a, the bright contrast phases are $MoSi_2$ and ZrB_2, while the dark regions consist of the SiC matrix. $MoSi_2$ and ZrB_2 give rise to a very similar contrast under SEM analysis and therefore they cannot be distinguished except by EDS analysis (Fig. 4b). Despite the differences in thermal expansion coefficient between the phases present, no microcracks were observed at the boundaries between the inclusions and the matrix. Good adhesion was also found between the $MoSi_2$ and ZrB_2 particles (Fig. 4b). $MoSi_2$ and ZrB_2 grains tend to form large agglomerates, with mean dimensions of ~5 μm or even larger. This indicates that the dispersion and deagglomeration of these particles was not optimized. The SiC matrix has the same microstructural features of the reference material, i.e. preferentially rounded SiC grains separated by intergranular silicate films and the presence of secondary phase at triple points. The intergranular phase among adjacent SiC grains (see Fig. 4b) was based on Si–Al–O or Y–Si–Al–O elements, such as in the baseline material. The SiC mean grain size is

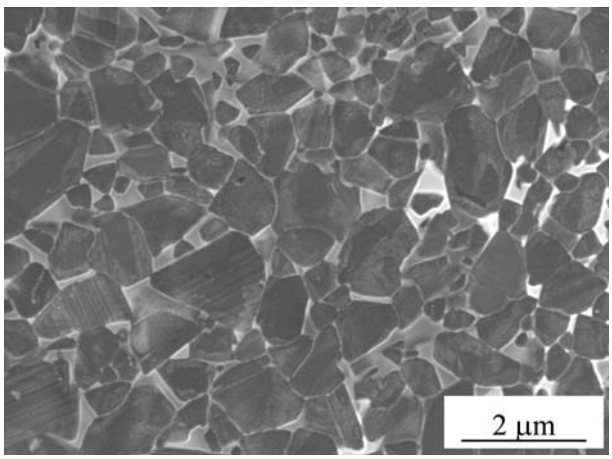

Fig. 1 Microstructure of polished and plasma etched section of SAY reference material

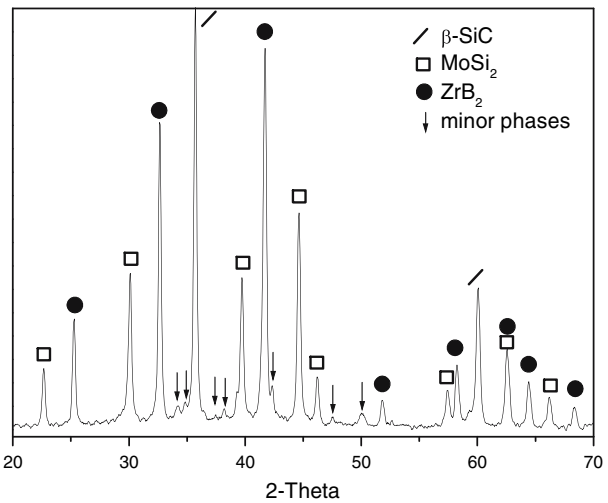

Fig. 2 X-ray diffraction pattern of the composite SZM

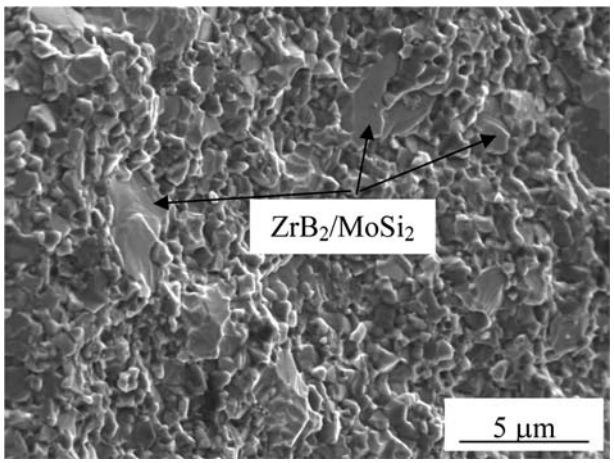

Fig. 3 Fracture surface of SZM composite

considerably reduced in comparison with the starting reference material (~300–400 nm) (Fig. 4b). This reduction is probably due to two concurrent factors. One is the reduced sintering time at the maximum temperature during the hot-pressing cycle for SZM, in comparison with the baseline material. The second is the presence of the hard particles, which are generally recognized to hinder the matrix grain boundary movement.

Mechanical properties

The measured values of mechanical properties are reported in Table 2. A high value of hardness (>22 GPa) was measured for the reference material. The hardness of the composite was not significantly different from the reference material. The addition of a relatively soft phase such as $MoSi_2$ (11 GPa [19]) was counterbalanced by the presence of ZrB_2, which has quite a high hardness (~24 GPa).

The Young's modulus was higher in the composite with respect to the reference SiC material, due to the high stiffness of the reinforcing phases. The theoretical bounds for the Young's modulus of a three-phase composite can be calculated by means of the relationships proposed by Hashin and Shtrikman and generalized by Walpole [20]. Considering the initial nominal composition of the materials and taking 386 GPa (Table 2) and 0.19 [21] as Young's modulus and Poisson coefficient for the SAY reference material, respectively, 440 GPa and 0.15 for $MoSi_2$ [22], 500 and 0.11 for ZrB_2 [23], the lower and upper bounds for material SZM are 411.6 GPa and 411.9 GPa, respectively, which are in very good agreement with the experimental value.

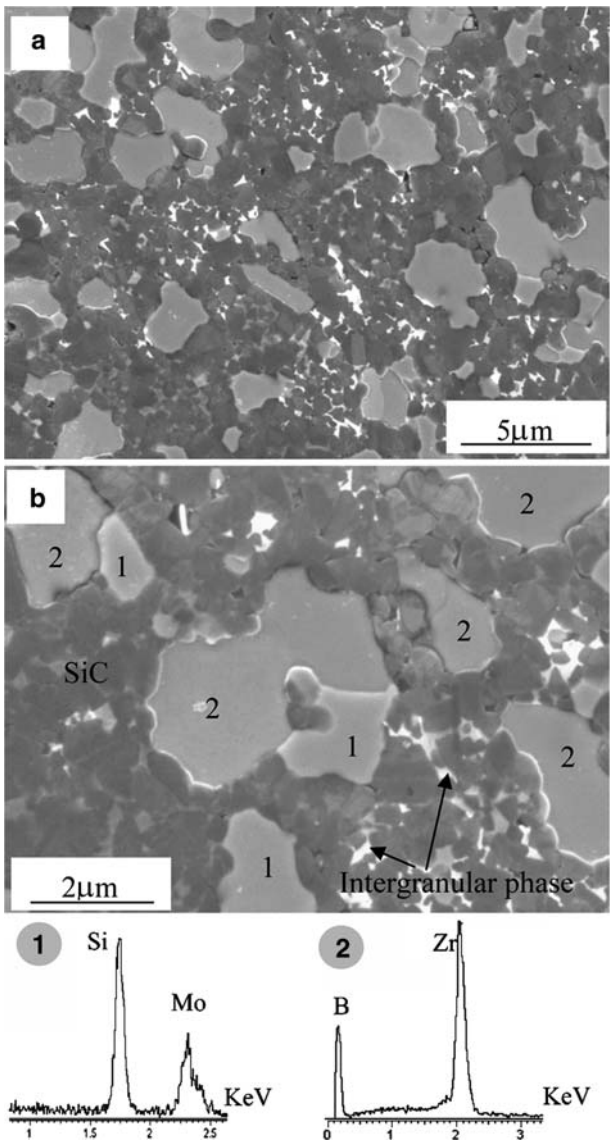

Fig. 4 Polished sections of sample SZM (**a**) Panoramic view of the composite, (**b**) detailed view, showing the refined SiC microstructure and an example of interface between $MoSi_2$ and ZrB_2 phase and relative EDS spectra

The fracture toughness of liquid-phase-sintered SiC-based materials with equiaxed morphology is not very high. Cracks, in fact, propagate mainly along grain boundaries without being appreciably deviated by the

Table 2 Mechanical properties and electrical properties of the materials produced

	HV GPa	E GPa	K_{Ic} MPa $m^{1/2}$	σ_{RT} MPa	$\sigma_{1,000\ °C}$ MPa	$\sigma_{1,300\ °C}$ MPa	ρ Ω cm
SAY	22.0 ± 0.8	386 ± 4	3.7 ± 0.3	746 ± 46	509 ± 34	148 ± 12	8.2
SZM	21.5 ± 0.6	412 ± 4	4.2 ± 0.2	856 ± 68	442 ± 22	141 ± 1	2.2×10^{-3}

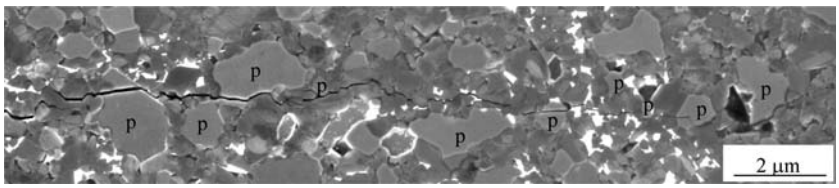

Fig. 5 Crack propagation generated by a Vickers indent with a 98.1 N load in SZM. ''p'' stands for ''particle'' and refers to $MoSi_2$ or ZrB_2 phase indifferently

equiaxed grain morphology. In the reinforced composite, there was a limited increase of toughness (+14%), which is due to toughening mechanisms activated by the reinforced particles. The most important mechanisms which are likely to occur in this composite are residual stresses [24], due to the difference in CTE between the reinforcing particles (9.1×10^{-6}/°C and 7.4×10^{-6}/°C for $MoSi_2$ [21] and ZrB_2 [23], respectively) and the SiC matrix (5.1×10^{-6}/°C [21]) and crack deflection. Analysis of the fracture surface evidenced that small particles tend to deflect the crack along the interface with the matrix, whilst the large particles or agglomerates are generally crossed by the crack and do not act as deflecting agents. An example of the crack path generated by a 98.1 N Vickers indent is shown in Fig. 5. It is very likely that a further improvement of the fracture toughness could derive from optimization of the powders' dispersion and homogenization, avoiding the formation of large agglomerates.

The room-temperature strength values of the SiC reference material were quite high (about 750 MPa). A good strength (up to 500 MPa) was maintained up to ~1,000 °C while it strongly decreased to values lower than 200 MPa at 1,300° C. This strong deterioration was due to softening of the amorphous intergranular phase at elevated temperatures.

In the reinforced composite, there was further improvement of the room-temperature strength in comparison with the reference material. This improvement is probably related to the increase in the fracture toughness (see Table 2). At 1,000 and 1,300 °C, there is almost no difference between the strength of the two materials produced. Since the chemistry of the SiC intergranular phase is not modified by the introduction of the electroconductive phases, it is concluded that the drop in strength at high temperature in SZM is due to softening of the amorphous silica-based intergranular phase, such as in the monolithic material.

The electrical resistivity of the composite is more than three orders of magnitude lower than that of the SiC reference material (Table 2), as a result of interconnectivity of the electroconductive particles.

The results presented show that the addition of $MoSi_2$ and ZrB_2 is effective for obtaining an electroconductive SiC-based material. The room-temperature properties benefit from the synergy of properties of each constituent phase. These added phases, however, do not significantly improve the high-temperature strength in comparison with the SiC baseline material.

Conclusions

An almost fully dense electroconductive SiC-based composite containing 14 vol% of $MoSi_2$ and ZrB_2 particles was sintered by hot pressing. The comparison with an SiC reference material highlights that the addition of particulate resulted in a slight improvement in the sinterability of the system.

The reinforcing particles do not react with the SiC phase and show good adhesion with the matrix. The composite contains an intergranular phase, whose chemistry is very close to that of the reference SiC material, containing silicate phases and partially crystalline, partially amorphous YAG. The room-temperature mechanical properties are generally improved with respect to the baseline material. The fracture toughness is increased by 14%, the room-temperature strength by 15%. The high-temperature strength experiences the same degradation of the reference materials, which is governed by softening of the secondary phases. The composite electrical resistivity is 2.2×10^{-3} Ω·cm.

References

1. Van Dijen FK, Mayer E (1996) J Eur Ceram Soc 16:413
2. Dressler EW, Riedel R (1997) Int J Refractory Metals Hard Mater 15:13
3. Falk LK (1997) J Eur Ceram Soc 17:983
4. Sciti D, Bellosi A (2000) J MatSci 35:3849
5. Balbo A, Dalle Fabbriche D, Sciti D, Bellosi A (2004) In: Mandal H, Öveçoğlu L (eds) Key engineering materials, vols 264–268. Trans Tech Publications, Switzerland, p 1039
6. Gomez E, Echeberria J, Iturriza I, Castro F (2004) J Eur Ceram Soc 24:2895
7. Sciti D, Balbo A, Bellosi A (2005) Adv Eng Mat 7:152
8. Petrovic JJ, Pena MI, Reimanis IE, Sandlin MS, Conzone SD, Kung HH, Butt DP (1997) J Am Ceram Soc 80:3070
9. Petrovic JJ, Honnel RE (1990) J Mater Sci Letts 9:1083
10. Sciti D, Guicciardi S, Melandri C, Bellosi A (2003) J Am Ceram Soc 86:1720
11. Klemm H, Tangermann K, Schubert C, Hermel W (1996) J Am Ceram Soc 79:2429
12. Medri V, Bellosi A (2004) J Mater Res 19:1567
13. Krnel K, Sciti D, Landi E, Bellosi A (2003) Appl Surf Sci 210:274
14. Mizutani T, Tsuge A (1992) J Ceram Soc Jpn Int Ed 100:979

15. Munz DG, Shannon JL Jr, Bubsey RT (1980) Int J Fracture 16:137
16. Mulla MA, Kristic VK (1991) Ceram Bull 70:439
17. Levin EM, Robbins CR, Mc Murdie HF (1969) Phase diagram for ceramists, 1969 Suppl. The American Ceramic Society, Columbus, OH, p 98
18. Roebben G, Sardu C, van der Biest O (2003) In: Brito ME, Lin HT, Plucknett K (eds) Ceramic transactions: ''silicon based structural ceramics for the new millennium'', vol 142. The American Ceramic Society, Westerville, Ohio, p 123
19. Newmann A, Jewett T, Sampath S, Bernt C, Herman H (1998) J Mat Res 13:2662
20. Walpole LJ (1966) J Mech Phys Solids 14:151
21. Shackelford JF, Alexander W (eds) (2001) CRC Materials science and engineering handbook. CRC Press, USA
22. Nakamura M, Matsumoto S, Hirano T (1990) J Mat Sci 29:3309
23. Cutler RA (1991) In: Schneider SJ (ed) Engineered Materials Handbook, Ceramic and Glasses, vol 4. ASM International, The Materials Information Society, Materials Park, OH, p 787
24. Taya M, Hayashi S, Kobayashi AS, Yoon HS (1990) J Am Ceram Soc 73:1382